HHS Public Access

Author manuscript

Acta Physiol (Oxf). Author manuscript; available in PMC 2018 February 01.

Published in final edited form as:

Acta Physiol (Oxf). 2017 February ; 219(2): 521–536. doi:10.1111/apha.12742.

Claudin-2-mediated cation and water transport share a common pore

Rita Rosenthal[1], **Dorothee Günzel**[1], **Susanne M. Krug**[1], **Jörg-Dieter Schulzke**[1], **Michael Fromm**[1], and **Alan S.L. Yu**[2]

[1]Institute of Clinical Physiology, Department of Gastroenterology, Infectious Diseases and Rheumatology, Campus Benjamin Franklin, Charité – Universitätsmedizin Berlin, 12200 Berlin, Germany

[2]Division of Nephrology and Hypertension, and the Kidney Institute, University of Kansas Medical Center, Kansas City, KS 66160, USA

Abstract

Aim—Claudin-2 is a tight junction protein typically located in “leaky” epithelia exhibiting large paracellular permeabilities like small intestine and proximal kidney tubule. Former studies revealed that claudin-2 forms paracellular channels for small cations like sodium and potassium and also paracellular channels for water. This study analyzes whether the diffusive transport of sodium and water occurs through a common pore of the claudin-2 channel.

Methods—Wild-type claudin-2 and different claudin-2 mutants were expressed in MDCK I kidney tubule cells using an inducible system. Ion and water permeability and the effect of blocking reagents on both were investigated on different clones of the mutants.

Results—Neutralization of a negatively charged cation interaction site in the pore with the mutation, D65N, decreased both, sodium permeability and water permeability. Claudin-2 mutants (I66C and S68C) with substitution of the pore-lining amino acids with cysteine were used to test the effect of steric blocking of the claudin-2 pore by thiol-reactive reagents. Addition of thiol-reactive reagents to these mutants simultaneously decreased conductance and water permeability. Remarkably, all experimental perturbations caused parallel changes in ion conductance and water permeability, disproving different or independent passage pathways.

Conclusion—Our results indicate that claudin-2-mediated cation and water transport are frictionally coupled and share a common pore. This pore is lined and determined in permeability by amino acid residues of the first extracellular loop of claudin-2.

Corresponding authors: Alan S.L. Yu, Division of Nephrology and Hypertension, and the Kidney Institute, University of Kansas Medical Center, Kansas City, KS 66160, USA, phone: +1-913-588-9252, FAX: +1-913-588-9251, ayu@kumc.edu. Rita Rosenthal, Institute of Clinical Physiology, Campus Benjamin Franklin, Charité Berlin, 12200 Berlin, Germany, phone: +49-30-8445-2792, FAX: +49-30-8445-4239, rita.rosenthal@charite.de.

Declaration

The authors declare that they have no conflict of interest.

The authors confirm that the material submitted is conform with Good Publishing Practice in Physiology 2013: Guidelines for Acta Physiologica (Persson PB, 2013).

Keywords

Claudin-2 pore; paracellular transport; common pore for sodium and water

Introduction

Epithelia like those of kidney proximal tubule and small intestine are called ‘leaky’ because their paracellular pathway is more conductive for ions than their transcellular pathway. Therefore, ions are transported across these epithelia via both, transcellular and paracellular pathways. Whether or not a similar distribution also exists for water transport was debated controversially for decades. While the transcellular pathway for water via aquaporin channels has been well established more than 20 years ago (Agre *et al.* 1993), several pieces of evidence suggest that there is also a paracellular contribution to transepithelial water transport, at least in the proximal tubule (Schafer, 1990). At that time, however, the molecular basis of this pathway was unknown. More recently, the tight junction protein claudin-2, which is highly expressed in the proximal tubule, was identified as a paracellular water channel (Rosenthal *et al.* 2010).

Claudin-2 has been known for several years before to form a paracellular cation channel and to produce a distinct paracellular permeability for small cations (Amasheh *et al.* 2002). Claudin-2 overexpression does not affect the paracellular permeability for larger molecules like mannitol (184 Da) or lactulose (342 Da) (Amasheh *et al.* 2002). In contrast, other channel-forming claudins in the kidney such as the cation-permeable protein claudin-10b (Günzel *et al.* 2009) and the anion-permeable protein claudin-17 (Krug *et al.* 2012), are not permeable to water, indicating that specific characteristics of the pore are essential for concomitant ion and water transport. The relative permeability of claudin-2 to alkali metal cations follows a high-order Eisenman sequence and exhibits a very narrow ratio of permeabilities between the most-permeable and the least-permeable cation, suggesting that cations traverse the pore in a partially hydrated form (Eisenman and Horn, 1983, Nightingale, 1959). Consistent with this, the pore diameter of claudin-2 was estimated to be between 6.5 Å (Yu *et al.* 2009) and ~8 Å (Van Itallie *et al.* 2008) which appears large enough to allow the passage of partially hydrated cations and water molecules with a molecular diameter of about 2.8 Å. In the initial study of claudin-2-mediated water permeability, paracellular water flux across layers of claudin-2-expressing cells could be induced by a Na^+ gradient and conversely an osmotic gradient caused a paracellular Na^+ flux indicating that Na^+ and water flux are loosely coupled. Interestingly, the transport ratio of Na^+ and water was estimated to be much higher than that of hydrated Na^+ (Rosenthal *et al.* 2010).

For the most part, transcellular transport of solutes and of water occur through distinct and independent pathways. In this study, we tested the hypothesis that paracellular transport of Na^+ and water occurs through the *same* pathway and that this is mediated by a common pore in claudin-2. The hypothesis is made likely if a coupling between paracellular Na^+ and water movement is found and provide a mechanistic basis for electrokinetic phenomena, such as electroosmosis and streaming potentials.

Water flux measurements were performed on a high-resistance strain of Madin-Darby canine kidney (MDCK) cells with inducible expression of wild-type claudin-2 and different claudin-2 mutants. The mutations were in amino acid residues in the first extracellular loop (ECL) of claudin-2, which is known to line the paracellular pore of claudins (Colegio *et al.* 2002, Colegio *et al.* 2003, Van Itallie *et al.* 2003). It was previously shown that a negatively charged site within the first ECL formed by aspartate-65 causes the cation selectivity by electrostatic interaction. Neutralization of this amino acid residue by substitution with asparagine (D65N) caused a reduction in Na^+ permeability and hence a reduction in conductance in the transfected cells (Yu *et al.* 2009). In addition, two other pore-lining amino acid residues in the first ECL, I66 and S68, had previously been mutated to cysteine (Angelow and Yu, 2009, Li *et al.* 2014). Na^+ permeability of these claudin-2 mutants (I66C, S68C) was not changed compared to wild-type claudin-2, but the pore could be blocked by specific methanethiosulfonate reagents, which bound to the cysteines and decreased paracellular cation permeability of cells transfected with these cysteine mutants. Examination of water transport using these different claudin-2 mutants provided novel insights into the mechanism of paracellular claudin-2-mediated water permeability.

Material and Methods

Cell cultures

Experiments were performed on MDCK I TetOff claudin-2 cell lines expressing wild-type (wt) or mutant claudin-2. Cell lines were generated by methods described previously (Angelow and Yu, 2009, Yu *et al.* 2009). In brief, mutants of mouse claudin-2 were generated by site-directed mutagenesis using the QuikChange kit (Stratagene). cDNA of wt or mutant mouse claudin-2 were ligated into the retroviral Tet response vector. Retrovirus encoding claudin-2 was produced, transduced into MDCK I Tet-Off cells, and stable clones were selected using hygromycin (Angelow *et al.* 2007). The cells were grown in 25-cm^2 culture flasks containing MEM-EARLE (PAA Laboratories GmbH, Pasching, Austria) supplemented with 10% (v/v) fetal bovine serum, 100 mg/ml streptomycin, 100 U/ml penicillin (Biochrom AG, Berlin, Germany), and 300 μg/ml hygromycin (PAA Laboratories GmbH, Pasching, Austria). The cells were cultured in presence of 20 ng/ml doxycycline to suppress claudin-2 expression (Dox+). For induction of claudin-2 expression, doxycycline was omitted from the culture medium starting from the day of seeding (Dox−). Cells were cultured at 37°C in a humidified 5% CO_2 atmosphere. For water flux measurements and electrophysiological studies cell monolayers were cultured on porous culture plate inserts (Millicell PCF filters, pore size 0.4 μm, effective area 0.6 cm^2, Millipore GmbH, Schwalbach, Germany) for 7 to 9 days before they were used for experiments. Cells were screened for claudin-2 expression by Western blot analysis and immunofluorescence staining in combination with confocal laser scanning microscopy to confirm the localization of claudin-2 within the tight junction (see below). Two clones of cells expressing wild-type, D65N and I66C claudin-2 and one clone of cells expressing S68C claudin-2 were tested in this study.

Western blot analysis

Western blot analysis was performed as reported (Amasheh *et al.* 2002). Cells grown on culture plate inserts were scraped and homogenized in lysis buffer containing 20 mM TRIS, 5 mM $MgCl_2$, 1 mM EDTA, 0.3 mM EGTA, and 1x complete protease inhibitor mixture (Roche, Mannheim, Germany), and passaged through a 26 G 1/2 needle. The membrane fraction was obtained as pellet after two centrifugation steps. The protein concentration of the resuspended pellet was determined by the BCA method (Pierce, Perbio Science GmbH, Bonn, Germany), and quantification with a plate reader (Tecan Deutschland GmbH, Crailheim, Germany). Protein samples were separated by SDS-polyacrylamide gel electrophoresis and blotted onto a PVDF-membrane for detection of tight junction proteins and aquaporins. After blocking with BSA and incubation of membranes with primary antibodies (anti-claudin, anti-occludin from Invitrogen, Carlsbad, CA; anti-AQP from Santa Cruz, Dallas, TX; anti-β-actin from Sigma-Aldrich, St Louis, MO), chemiluminescence was induced with a Lumi-LightPLUS Western blotting kit (Roche, Mannheim, Germany) and detected with an LAS-1000 imaging system (Fuji, Tokyo, Japan). β-actin staining served as loading control.

Immunofluorescence analysis

Immunofluorescence studies were performed with cells grown on culture plate inserts. Confluent monolayers were rinsed with phosphate-buffered saline (PBS), fixed with 2% PFA, permeabilized with PBS containing 0.5% (v/v) Triton X-100, and incubated in blocking solution (1% goat serum, 6% BSA in PBS). Then, monolayers were stained with primary polyclonal antibody against claudin-2 and monoclonal antibody against occludin (both used at concentrations of 20 μg/ml, Invitrogen), followed by labeled secondary antibody (Alexa Fluor 488 goat anti-mouse IgG and Alexa Fluor 594 goat anti-rabbit IgG, both used at concentrations of 2 μg/ml, Invitrogen), and mounted in ProTaqs Mount Fluor (BIOCYC, Luckenwalde, Germany). Fluorescence images were obtained with a confocal laser scanning microscope (Zeiss LSM 510 META, Jena, Germany) at excitation wavelengths of 543 and 488 nm.

Dilution potential measurements

Dilution potential measurements for determination of Na^+ and Cl^- permeabilities were performed in Ussing chambers modified for cell culture inserts. Water-jacketed gas lifts were filled with 10 ml circulating fluid on each side. Bath solution contained (in mM) 119 NaCl, 21 $NaHCO_3$, 5.4 KCl, 1.2 $CaCl_2$, 1 $MgSO_4$, 3 HEPES, 10 D(+)-glucose and was gassed with 95% O_2 and 5% CO_2 to ensure a pH value of 7.4 and the temperature was kept at 37°C. To determine ion permeabilities, 5 ml of the standard bath solution on either the apical or the basolateral side of the cell layer was replaced by a solution containing 238 mM mannitol instead of 119 mM NaCl. Resulting potentials were corrected for liquid junction potentials which were determined in analogous experiments using empty cell culture inserts, using the PNa/PCl ratio calculated from the Goldman-Hodgkin-Katz equation and the transepithelial resistance measured during the same experiment (Kimizuka and Koketsu, 1964). All data were corrected for filter resistance.

Measurement of transepithelial water permeability

To measure water permeability, a modified Ussing chamber was used as described recently (Rosenthal *et al.* 2010). During water flux measurements, transepithelial resistance (TER, $\Omega \cdot cm^2$), short-circuit current (I_{SC}, $\mu A \cdot cm^{-2}$), and transepithelial voltage (mV) were recorded by a standard PC with ADC-DAC cards. Resistance of bathing solution and blank filter support was measured prior to each experiment and subtracted. The transepithelial voltage was clamped to 0 mV to avoid effects on ion and water flux. Stability of TER during the experiment was used as an indicator of cell viability.

Cell filters were mounted in Ussing chambers, and perfused with HEPES buffered solution with the following composition (in mM): 134.6 NaCl, 2.4 Na_2HPO_4, 0.6 NaH_2PO_4, 5.4 KCl, 1.2 $MgCl_2$, 1.2 $CaCl_2$, 10.6 HEPES, 10 D(+)-glucose, adjusted to pH = 7.4 with approximately 5 mM NaOH, thus, the total effective NaCl concentration was 144.8 mM. A rotary pump ensured constant circulation of the perfusion solution (2.8 ml/min) and thus a fast fluid exchange in both hemi-chambers (volume 500 µl) to avoid effects of unstirred layers on water permeability.

Water flux was induced by a transepithelial osmotic or ionic gradient. The experimental conditions and direction of fluxes are summarized in Fig. 1. (a) For experiments with an osmotic gradient alone, mannitol (100 mM) was added either in the apical (as shown here) or basolateral compartment of the Ussing chamber. Flux from the apical to the basolateral compartment was defined as negative flux. (b) For experiments with an ionic gradient (80 mM NaCl) with “osmotic compensation”, the NaCl solution in the apical compartment was lowered to 64.8 mM and kept at 144.8 mM in the basolateral compartment. 160 mM mannitol was added to the apical compartment to oppose the osmotic effect of the NaCl gradient. (c) Experiments with an ionic gradient “without osmotic compensation” were identical to (b) but without addition of mannitol to the apical compartment.

The fluid level in both tubes was monitored by a visual system ColorView XS (Olympus Soft Imaging Solutions GmbH), at time 0 min and every 10 min over a period of 120 min. Transepithelial water flux was calculated from the difference between the menisci at the registration times and given as water flux per square centimeter and hour. Claudin-2-mediated water flux was calculated as the difference between water flux of induced (Dox−) and uninduced (Dox+) cells. Water permeability was calculated from $P = J/\Delta c$ with P = permeability (cm/s), J = flux ($mol \cdot h^{-1} \cdot cm^{-2}$), and c = concentration (mol/l). For blocking experiments with methanethiosulfonate (MTS) reagents, water flux was measured over 120 minutes before the reagents were added and further 120 minutes in the presence of the reagents.

Freeze-fracture electron microscopy

Freeze-fracture analysis of cells grown on cell culture inserts was performed as described before (Rosenthal *et al.* 2010). Cells were fixed, frozen, fractured, and shadowed with platinum and carbon in a vacuum evaporator (Denton DV-502, Denton Vacuum, Cherry Hill, NJ). The obtained replicas were bleached with sodium hypochloride, fixed on copper grids, and investigated using a Zeiss 902A electron microscope (Carl Zeiss NTS, Oberkochen,

Germany) in combination with a digital camera iTEM Veleta (Olympus Soft Imaging Solutions, Münster, Germany).

Morphometric analysis was performed on coded prints of freeze-fracture electron micrographs (51,000 × magnification) of all TJ regions in which an apical and a contra-apical strand of the meshwork could be clearly differentiated. The meshwork depth was the distance between these strands. Vertical grids were drawn at 200 nm intervals perpendicular to the most apical TJ strand. The number of horizontal strands within the main TJ meshwork was counted at intersections with grid lines. Strand discontinuities within the meshwork were defined as 'breaks' when >20 nm and given per micrometer length of horizontal strands. The linearity of strand formation was specified as 'particle type' or 'continuous'.

Statistical Analysis

Data are expressed as means ± SEM. Statistical analysis was performed using unpaired Student's *t* test unless otherwise stated and the Bonferroni-Holm correction for multiple comparisons. A *p* value less than 0.05 was considered to be statistically significant. The number (n) refers to the number of experiments.

Results

Characterization of stable transfected MDCK I TetOff cells expressing wild-type and mutant claudin-2

MDCK I TetOff cells were stably transfected with mouse claudin-2, either wild-type (WT) or different mutants: the charge-neutralizing mutant D65N and two different cysteine mutants, I66C and S68C. Two different clones of wild-type, D65N and I66C and one clone of S68C expressing cells were analyzed. All cells exhibit inducible expression of claudin-2 in the absence of doxycycline (Dox−), which was completely suppressed in the presence of doxycycline (Dox+). Double immunofluorescence staining of Dox− cells using antibodies against claudin-2 and the tight junction protein occludin revealed a colocalisation of both proteins indicating a localization of wild-type and all claudin-2 mutants at the tight junction, with some additional intracellular staining (Fig. 2a). The analysis of endogenous claudin expression in the transfected cells revealed variability in protein expression between the different clones used in the study, but no differences between Dox− and Dox+ cells could be detected so that changes in the paracellular permeability of induced cells are most likely attributable to the presence of claudin-2 within the tight junction (Fig. 2b). Furthermore, the expression of claudin-2 did not affect the expression of the AQP water channels, AQP1, AQP3, and AQP4, which are predominantly expressed in MDCK I cells (Fig. 2b), so that differences in transepithelial water flux are unlikely to be caused by changes in transcellular water flux and can be assumed to be due to changes in paracellular water flux.

Comparison of cells expressing wild-type and the charge-neutralizing mutant D65N of claudin-2

Transfected cells induced to express claudin-2 (Dox−) showed an increase in transepithelial conductance which was due to an increase in Na^+ permeability (Fig. 3) compared to uninduced (Dox+) cells. A comparison between induced cells expressing wild-type

claudin-2 and the mutant D65N with the charge-neutralizing mutation in the first extracellular loop revealed a decreased conductance as a result of the decreased Na^+ permeability in cells with the mutant claudin-2 (Fig. 3a, b). Water flux across the layer of induced cells expressing wild-type claudin-2 was increased compared to the uninduced cells both with an osmotic gradient with 100 mM mannitol (Fig. 4a) and an ionic gradient in the absence of any osmotic gradient (Fig. 4b). For induction of water flux by an ionic gradient, a basolateral to apical NaCl gradient (80 mM) was used and 160 mM mannitol was added to the apical solution for "compensation" of the osmotic difference. In contrast to wild-type claudin-2-expressing cells, no differences between uninduced and induced cells could be observed in cells transfected with the D65N mutant of claudin-2. Under both osmotic and ionic gradients, water flux across the layer of cells expressing wild-type claudin-2 was higher than in cells expressing the D65N claudin-2 mutant. No differences between uninduced (Dox+) wild-type and D65N cells could be observed under any conditions. Measuring water transport in the presence of the 80 mM NaCl gradient without osmotic compensation with mannitol showed no differences between induced and uninduced wild-type and D65N claudin-2-expressing cells (Table 1). Under these conditions, the concentration gradient is directed from basolateral to apical, and the osmotic gradient is in the opposite direction.

To analyze whether changes in tight junction ultrastructure cause the differences in water transport between uninduced and induced cells and between wild-type and D65N claudin-2 expressing cells, freeze-fracture electron microscopy studies were performed. No differences in relative occurrence and number of tight junction strands, meshwork depth, density of bicellular tight junction strands, and the number of breaks in the tight junction strands could be detected, neither between induced and uninduced cells nor between wild-type claudin-2- and D65N claudin-2-transfected cells (Table 2, Fig. S1). As already shown in another study on MDCK I cells overexpressing claudin-2 (Furuse *et al.* 2001) we found a shift from continuous-type strands to particle-type strands when wild-type or D65N claudin-2 was expressed in the cells which is due to a stronger association to the E-face and correlates with the tightness of individual tight junction strands.

Analysis of cells expressing cysteine mutants of claudin-2

Cells induced to express the cysteine mutants I66C or S68C of claudin-2 showed an increase in conductance (Fig. 5a) due to the increase in Na^+ permeability (Fig. 5b) compared to the uninduced cells. Na^+ permeability and conductance of some clones differed slightly from that measured for wild-type claudin-2-expressing clones, which could be due to clone-dependent variability in claudin-2 expression. It has been shown that the pore properties of claudin-2 are not affected in I66C, suggesting that this amino acid residue in the first ECL is not directly involved in the mechanism of ion permeation. Water flux across these epithelial monolayers under osmotic conditions revealed an increased flux in the induced cells (Fig. 5c).

To analyze whether the modification of the paracellular pores of claudin-2 exerts any effect on water flux, water flux was measured before and after addition of methanethiosulfonate (MTS) reagents (Fig. 6). It has been shown that the pore of I66C claudin-2 could be blocked

by MTSEA ((2-aminoethyl)methanethiosulfonate) or MTSET ([2-(trimethylammonium) ethyl]methanethiosulfonate, whereas MTSES ((2-sulfonatoethyl) methanethiosulfonate) has no blocking effect (Yu *et al.* 2009). Addition of MTSEA (2.5 mM) or MTSET (1.0 mM) to the induced I66C claudin-2 transfected cells resulted in a decrease in transepithelial water flux which is associated with a decrease in conductance (Fig. 6a). In contrast, MTSES (5 mM) had neither an effect on transepithelial water flux nor on conductance. The inhibitory effect of MTSEA and MTSET on water flux and conductance was confirmed on a second clone of I66C-expressing cells (#35) and on cells expressing the S68C mutant (Li *et al.* 2014) (Fig. 6b). The inhibition of both parameters by MTS reagents was stronger in cells expressing the S68C mutant compared to the I66C mutant.

Both reagents, MTSEA and MTSET, did not change water flux across layers of the corresponding uninduced cells (Fig. 6c), so the transcellular water flux mediated by aquaporin water channels was not affected by MTS reagents. Moreover, no effect of MTSEA and MTSET on conductance could be detected in Dox+ cells (Fig. 6c), confirming that these reagents modulate exclusively the conductance of claudin-2 and not of endogenous tight junction proteins or transcellular transport proteins.

Relationship between claudin-2-mediated water permeability and ion conductance

To analyze the specific characteristics of claudin-2, the values concerning conductance and water permeability obtained on the induced (Dox−) cells were corrected for the base-line values obtained with uninduced (Dox+) cells. The results represent the permeability attributable to the claudin-2 pore itself (Fig. 7). For the cysteine mutants, the values in absence and presence of the MTS reagents were calculated. With the exception of S68C, the data show an approximately linear correlation between conductance, which represents ion permeability (and in case of our experimental conditions and claudin-2 mainly Na^+ permeability), and water permeability. In cells expressing the S68C mutant of claudin-2, water flux was disproportionately larger compared to cells expressing wild-type claudin-2 or the other claudin-2 mutants. Additionally, the inhibitory effect on water permeability caused by the MTS reagents was stronger in S68C than in I66C.

Discussion

The present study confirms that claudin-2 mediates paracellular water transport. Furthermore, it shows that a decreased Na^+ permeability is associated with decreased water permeability and that steric blocking of the paracellular cation pore results in decreased water permeability. These findings indicate that Na^+ and water share the same pore and suggest that their transport within the pore is loosely coupled. The permeability of claudin-2 for Na^+, K^+, and other monovalent cations is very similar (Yu *et al.* 2009, Rosenthal *et al.* 2010).

Claudin-2 was previously shown to be permeable to water in an overexpression study on a cell culture model, using high-resistance MDCK C7 cells that lack endogenous expression of claudin-2 (Rosenthal *et al.* 2010). Here, the overexpression study was confirmed in an inducible cell system based on the high-resistance cell line MDCK I. By using an inducible clonal cell line, the uninduced cells act as an isogenic negative control, thus eliminating

errors due to clonal variability. This also allowed us to subtract the conductance as well as the Na^+ and water permeability in the induced state from that in the uninduced state and thus deduce the permeability of a single claudin, here claudin-2 (Fig. 7). Prerequisite for this is that no differences in endogenous claudin expression between Dox− and Dox+ cells exist, which could be confirmed by Western blot analysis. However, the transfected cells revealed variability in protein expression between the different clones used in the study, but these differences does not seem to affect the Na^+ and water permeability since the values of the uninduced cells of different clones are very similar. Furthermore, this study confirms that solute polarization within the lateral intercellular spaces did not contribute to osmotically induced water flux and thus to differences between Dox− and Dox+ cells. Water flux induced by mannitol was independent of the direction of the osmotic gradient, as shown in Dox− and Dox+ cells expressing wild-type claudin-2 or the I66C mutant (Table 1). Application of mannitol to the apical or basolateral side of the cells resulted in water fluxes with opposite direction, but the absolute fluxes were equal.

Na^+ and water permeate the same pore

The cation pore in claudin-2 is lined by residues of the first ECL and has a diameter of approximately 6.5 Å (Yu *et al.* 2009), which is large enough to allow the passage of partially hydrated cations and water molecules. Our previous observation that a NaCl gradient could drive water flux under isoosmotic conditions already suggested the possibility that Na^+ and water might permeate through a common pore in claudin-2 (Rosenthal *et al.* 2010). Our current experiments now provide persuasive evidence of this. Here we use cysteine mutants of the cation pore-lining first ECL amino acids, I66 and S68 (Angelow and Yu, 2009, Li *et al.* 2014), to study the effect of blocking the claudin-2 cation pore with different MTS reagents. MTS reagents bind covalently to the substituted cysteines but not to the two endogenous cysteines in the first ECL, because the latter are connected by an intramolecular disulfide bond and therefore are not accessible (Li *et al.* 2013b). It has been shown that MTS reagents cause a partial inhibition of Na^+ permeability and conductance in these mutants. We found that application of the MTS reagents, MTSEA (236 Da) and MTSET (278 Da), strongly inhibited both conductance and water permeability in cells expressing the I66C and S68C mutant, whereas MTSES (219 Da) had no effect on either conductance or water permeability. These findings are consistent with the idea that Na^+ and water permeate through the same pore. Additional evidence in support of this is our finding that a mutation that increases the cation pore diameter also increases water permeability (see discussion below).

Na^+ and water flux are coupled within the claudin pore

The passage of Na^+ and water through the claudin pore could occur in one of two ways: (i) Na^+ and water could permeate independently of each other within the same pore, or (ii) Na^+ and water could interact within the pore in such a way that their movement is frictionally “coupled”. Three lines of evidence support a model of frictional coupling. First, we have already shown that a Na^+ gradient can drive water flux (Rosenthal *et al.* 2010). Second, we now show that the mutation, D65N, which reduces Na^+ permeability by eliminating a negatively charged interaction site within the pore without affecting its diameter (Yu *et al.* 2009, Li *et al.* 2013a), also concomitantly reduces water flux. Since it is unlikely that

replacement of a charged residue with a polar residue would directly reduce water permeation through the pore, the most plausible explanation for this is that Na^+ flux couples water movement along with it. Third, we find a linear correlation between conductance (which reflects Na^+ permeability) and water flux (or water permeability) across different claudin-2 mutants and different clonal lines, and regardless of the absence or presence of a pore-blocking reagent (Fig. 7). The linear correlation exists for water flux induced by an osmotic gradient or an ionic gradient. The R^2 value is lower for water flux induced by an osmotic gradient due to the S68C mutant which seems to have a disproportionately high water flux maybe due to a slightly larger pore diameter (see below).

Analysis of the NaCl reflection coefficient

We were able to reach strikingly similar conclusions to those described above by taking a formal, thermodynamic approach. The osmotic water flux, J_V (basolateral-to-apical), is related to the water permeability of the monolayer, P_{water} (cm/s), the reflection coefficients, σ, of mannitol and NaCl and their concentration differences, Δ[X] (apical concentration minus basolateral concentration), by the Staverman correction of the van't Hoff equation (Durbin, 1960):

$$J_V = P_{water} \left(\sigma_{NaCl.\Delta}[NaCl] + \sigma_{Mannitol}\,\Delta[Mannitol]\right)$$

In the osmotic gradient-driven water flux experiment, 100 mM mannitol was added apically with symmetrical NaCl concentrations (Δ[NaCl] = 0). The water flux in this situation is given by:

$$J_{VMannitol} = P_{water} \left(\sigma_{Mannitol}\,\Delta[Mannitol]\right)$$

Under these conditions, we found a 61% reduction in water flux through D65N claudin-2 compared to wild-type claudin-2, which likely represents a 61% reduction in P_{water} since all the other factors remain constant. This is strikingly similar to the 56% reduction in conductance and 51% reduction in P_{Na} of D65N, again supporting a model of frictionally coupled transport of Na^+ and water.

In the ionic gradient-driven water flux experiment, the NaCl concentration on the apical side was reduced (145 mM basolateral, 65 mM apical) and mannitol added (160 mM) to balance the osmolarity. The water flux in this situation is given by:

$$J_{VNaCl} = 0.16\, P_{water} \left(\sigma_{Mannitol} - \sigma_{NaCl}\right)$$

The fact that J_{VNaCl} was positive (basolateral-to-apical flow) in wild-type claudin-2 in this situation indicates that $\boldsymbol{\sigma}_{Mannitol} > \boldsymbol{\sigma}_{NaCl}$. Given that claudin-2 is permeable to Na^+ but not to mannitol (Amasheh *et al.* 2002, Van Itallie *et al.* 2008), thus, $\sigma_{Mannitol}$ is 1, σ_{NaCl} is given by:

$$\sigma_{\mathrm{NaCl}}=1-\frac{\mathrm{J}_{\mathrm{VNaCl}}\,\Delta[\mathrm{Mannitol}]}{\mathrm{J}_{\mathrm{VMannitol}}\,0.16}$$

The calculated value for σ_{NaCl} is 0.446 for wild-type claudin-2. As claudin-2 is permeable to Na^+, but not to Cl^-, this finding indicates that Na^+ and water must share the same pore pathway. For claudin-2 D65N, the calculated σ_{NaCl} value was 0.759. This is consistent with the finding that J_V driven by a ionic gradient was 83% lower compared to wild-type claudin-2 whereas P_{water} was only 61% lower indicating an increase in σ_{NaCl}. This is also consistent with the idea that Na^+ and water share a common pore that is lined by first ECL residues.

Until now, there has been no study which measured the NaCl reflection coefficient of claudin-2. The rat proximal tubule has been modeled and used to predict the NaCl reflection coefficient of the tight junction in rat proximal tubule, yielding values ranging from 0.65 (Weinstein, 1984) to 0.0079 (Guo *et al.* 2003). The dual pathway model of Guo et al (Guo *et al.* 2003) divided the tight junction pathway into pores and slit breaks, the pores with a NaCl reflection coefficient of 0.153 and the large slit breaks with a NaCl reflection coefficient of 0.000226.

Interpreting our experiments in terms of osmotic theory and reflection coefficients is helpful in explaining the effect of the ionic gradient with “osmotic compensation” experiment (Fig. 1B). The ionic gradient of 80 mmol/l NaCl generates an effective osmotic gradient of 160 × 0.446 = 71 mOsm/l. Thus, addition of 160 mM mannitol apically can be viewed as creating a net osmotic gradient of 89 mOsm/l (160 mOsm/l - 71 mOsm/l) directed apically and driving water towards the apical compartment. This may explain that the magnitude of claudin-2-mediated water flux is similar in the presence of the osmotic gradient with 100 mM mannitol and the ionic gradient in combination with 160 mM mannitol.

The theory fails, however, to explain the results of our experiment using an ionic gradient without “compensation” (Fig. 1C). Interpreted in the light of osmotic theory, an isolated NaCl gradient should drive osmotic movement of water towards the basolateral compartment. Since the claudin-2-mediated water flux is zero, water movement appears to be obstructed, possibly by the ionic gradient or by a change in cell shape and closure of the lateral intercellular spaces. Alternatively, claudin-2-mediated water flux may be present but too small to be detected under these conditions due to the overlapping (transcellular) background water flux.

Calculating the coupling ratio of Na^+ to water from Na^+ and water permeability of claudin-2, we found values of about 1:30 for all clones of wild-type and mutant claudin-2 with exception of the S68C mutant with the larger pore diameter. For this claudin-2 mutant the coupling ratio was 1:78. These values indicate a water flux, which exceeded that of the first Na^+ hydration shell.

Effect of pore size on water permeability

Previous studies indicated that the pore diameters of wild-type claudin-2 (6.5 Å) and the claudin-2 mutants D65N (6.6 Å) and I66C (6.4 Å) are very similar, whereas the S68C mutant has a slightly larger pore diameter of 7.0 Å (Li *et al.* 2013a, Li *et al.* 2014). Other pore characteristics seem not to be affected in the mutants as indicated by the unchanged Eisenman sequence. For the S68C mutant we found (i) a higher water permeability than in wild-type and I66C claudin-2, when factored for conductance or Na^+ permeability, and (ii) a stronger inhibitory effect of the MTS reagents compared to I66C. The higher water permeability could be due to the increased pore diameter, which promotes the permeation of water molecules with a diameter of about 2.8 Å. An increase in pore diameter does not influence Na^+ permeability because the magnitude of this is determined primarily by the availability of negatively charged intrapore sites at D65 and Y67 for electrostatic interaction with dehydrated Na^+ (Yu *et al.* 2009, Li *et al.* 2013a). Since S68 is located at the narrowest part of the pore (Li *et al.* 2014), steric blocking at this position results in a higher degree of inhibition than at a position in a wider part of the pore. Application of MTSEA and MTSET both caused an approximately 35% inhibition of conductance in I66C mutants, compared to inhibition of 63% for MTSEA and 48% for MTSET in the S68C mutant. Inhibition of water flux averaged 23% for both MTS reagents in the I66C mutants and 58% with MTSEA and 51% with MTSET in the S68C mutant. These findings provide additional support for the hypothesis that Na^+ and water pass the tight junction through the same pore and that this pore is lined by the amino acid residues of the first ECL of claudin-2.

Using the σ_{NaCl} of 0.446 for calculating the radius of the claudin-2 pore R_{pore} according to the calculations of Guo *et al.* (Guo *et al.* 2003) and assuming an average radius of Na^+ and Cl^- of 1.47 Å, we obtained a value of 3.47 Å for R_{pore}, thus a diameter of 6.9 Å, which seems to be a good estimation compared to the data (6.5 Å) found in other studies (Li *et al.* 2013a, Li *et al.* 2014). A pore diameter of about 6.5 Å seems to be necessary for water permeability, since claudin-10b with a pore diameter of 6.1 Å (Li *et al.* 2013a) is permeable to cations, but impermeable to water (Günzel *et al.* 2009, Rosenthal *et al.* 2010).

Role of claudin-2 in the kidney

In the kidney, claudin-2 is exclusively expressed in the proximal nephron (Enck *et al.* 2001, Kiuchi-Saishin *et al.* 2002) where the majority of NaCl and water reabsorption occurs. In proximal tubule, water permeability is much higher than water permeability measured in the claudin-2 expressing MDCK I cells (Table 1) or water permeability of claudin-2 ($4.73\ 10^{-4}$ cm/s). For proximal tubule the values for water permeability varied from $35{\cdot}10^{-3}$ cm/s (Quigley and Baum, 1996) to $150{\cdot}10^{-3}$ cm/s (Schnermann *et al.* 1998), whereas the water permeability of MDCK I cells expressing wild-type claudin-2 is about $5{\cdot}10^{-4}$ cm/s. The cell culture model cannot be directly compared with the proximal tubule because of differences in the molecular composition of the tight junction, the tight junction extension, expression level of claudin-2 and aquaporins, which all contribute to the differences in transepithelial water permeability. For example, the TER value of claudin-2 expressing MDCK I cells (160 $\Omega{\cdot}cm^2$) is much higher compared with the proximal tubules (4.5 $\Omega{\cdot}cm^2$ (Melis *et al.* 1993) and 16 $\Omega{\cdot}cm^2$ (Bello-Reuss, 1986)).

The claudin-2 knockout mice generated by Muto showed a 30% decrease of net transepithelial reabsorption of Na^+, Cl^-, and water in isolated proximal tubules and loss of Na^+ selectivity (Muto *et al.* 2010). Schnermann and coworkers found a 23% decrease in proximal fluid reabsorption in claudin-2-deficient mice (Schnermann *et al.* 2013). These data point to an involvement of claudin-2 to proximal tubule water reabsorption. Nevertheless, the contribution of the claudin-2 water pathway to the paracellular water reabsorption in proximal tubule remains still unclear. Estimation of tight junction water permeability in rat proximal tubule based on a mathematical model yielded much higher values of P_f A=0.22·cm^3/s (Weinstein *et al.* 2007). Recently, a pore/slit model was proposed for the transport across the tight junction in rat proximal tubule which suggested that numerous small circular pores based on claudin-2 account only for 5%, the large slit breaks for 95% of paracellular water permeability (Guo *et al.* 2003). Freeze-fracture electron microscopy studies revealed 1–2 tight junction strands with large breaks in mouse proximal tubule (Claude and Goodenough, 1973, Muto *et al.* 2010). However, such breaks did not account for paracellular water permeability in the cell culture model. Freeze-fracture studies on MDCK I cells transfected with wild-type claudin-2 or D65N claudin-2 detected no differences in the number and size of breaks in the tight junction strands between induced and uninduced cells that could represent the slit breaks for water permeation. Also other parameters of tight junction ultrastructure were unchanged as already shown in the claudin-2 overexpression model (Rosenthal *et al.* 2010). The observed shift from continuous-type strands to particle-type strands in claudin-2-expressing cells indicated a lower association of tight junction strand particles to the P-face and correlated with the tightness of individual strands (Furuse *et al.* 2001). The linearity of tight junction strands seems to be not important for paracelluar water permeability, since we did not observe such change in MDCK C7 cells overexpressing claudin-2 with increased water transport (Rosenthal *et al.* 2010). Thus, paracellular water permeability measured in MDCK cells transfected with claudin-2 was mediated by the claudin-2 pore.

Since claudin-2 forms a channel that is selectively permeable for cations, an additional pathway is necessary for anion reabsorption. Recently, claudin-10a and claudin-17 have been identified as paracellular channels that are selective for anions (Van Itallie *et al.* 2006, Günzel *et al.* 2009, Krug *et al.* 2012). Both claudins are expressed in the proximal tubule (Kiuchi-Saishin *et al.* 2002, Van Itallie *et al.* 2006, Yu, 2015), so they are potential candidates to mediate paracellular Cl^- reabsorption in these segments. In contrast to claudin-2, the channels formed by claudin-10a (unpublished data) and claudin-17 (Krug *et al.* 2012) are not permeable to water.

In summary, this study shows that claudin-2-mediated water transport is dependent on Na^+ transport through claudin-2 and that both Na^+ and water share a common pore that is lined by specific amino acid residues from the first extracellular loop of claudin-2.

Supplementary Material

Refer to Web version on PubMed Central for supplementary material.

Acknowledgments

We would like to thank Detlef Sorgenfrei, In-Fah Lee, Britta Jebautzke, and Anja Fromm for their expert technical assistance, and Susanne Angelow and Jiahua Li who contributed to the creation and initial characterization of the cell lines.

This study was supported by the Deutsche Forschungsgemeinschaft [grant number FOR 721/2 TP 1] to M.F. and by the National Institutes of Health [grants R01DK062283 and U01GM094627] to A.Y.

References

Agre P, Preston GM, Smith BL, Jung JS, Raina S, Moon C, Guggino WB, Nielsen S. Aquaporin CHIP: the archetypal molecular water channel. Am J Physiol. 1993; 265:463–76.

Amasheh S, Meiri N, Gitter AH, Schöneberg T, Mankertz J, Schulzke JD, Fromm M. Claudin-2 expression induces cation-selective channels in tight junctions of epithelial cells. J Cell Sci. 2002; 115:4969–76. [PubMed: 12432083]

Angelow S, El-Husseini R, Kanzawa SA, Yu AS. Renal localization and function of the tight junction protein, claudin-19. Am J Physiol Renal Physiol. 2007; 293:166–77.

Angelow S, Yu AS. Structure-function studies of claudin extracellular domains by cysteine-scanning mutagenesis. J Biol Chem. 2009; 284:29205–17. [PubMed: 19690347]

Bello-Reuss E. Cell membranes and paracellular resistances in isolated renal proximal tubules from rabbit and Ambystoma. J Physiol. 1986; 370:25–38. [PubMed: 3958978]

Claude P, Goodenough DA. Fracture faces of zonulae occludentes from “tight” and “leaky” epithelia. J Cell Biol. 1973; 58:390–400. [PubMed: 4199658]

Colegio OR, Van Itallie C, Rahner C, Anderson JM. Claudin extracellular domains determine paracellular charge selectivity and resistance but not tight junction fibril architecture. Am J Physiol Cell Physiol. 2003; 284:1346–54.

Colegio OR, Van Itallie CM, McCrea HJ, Rahner C, Anderson JM. Claudins create charge-selective channels in the paracellular pathway between epithelial cells. Am J Physiol Cell Physiol. 2002; 283:142–7.

Durbin RP. Osmotic flow of water across permeable cellulose membranes. J Gen Physiol. 1960; 44:315–26. [PubMed: 13725178]

Eisenman G, Horn R. Ionic selectivity revisited: the role of kinetic and equilibrium processes in ion permeation through channels. J Membr Biol. 1983; 76:197–225. [PubMed: 6100862]

Enck AH, Berger UV, Yu AS. Claudin-2 is selectively expressed in proximal nephron in mouse kidney. Am J Physiol Renal Physiol. 2001; 281:966–74.

Furuse M, Furuse K, Sasaki H, Tsukita S. Conversion of zonulae occludentes from tight to leaky strand type by introducing claudin-2 into Madin-Darby canine kidney I cells. J Cell Biol. 2001; 153:263–72. [PubMed: 11309408]

Günzel D, Stuiver M, Kausalya PJ, Haisch L, Krug SM, Rosenthal R, Meij IC, Hunziker W, Fromm M, Müller D. Claudin-10 exists in six alternatively spliced isoforms that exhibit distinct localization and function. J Cell Sci. 2009; 122:1507–17. [PubMed: 19383724]

Guo P, Weinstein AM, Weinbaum S. A dual-pathway ultrastructural model for the tight junction of rat proximal tubule epithelium. Am J Physiol Renal Physiol. 2003; 285:F241–57. [PubMed: 12670832]

Kimizuka H, Koketsu K. Ion transport through cell membrane. J Theor Biol. 1964; 6:290–305. [PubMed: 5875308]

Kiuchi-Saishin Y, Gotoh S, Furuse M, Takasuga A, Tano Y, Tsukita S. Differential expression patterns of claudins, tight junction membrane proteins, in mouse nephron segments. J Am Soc Nephrol. 2002; 13:875–86. [PubMed: 11912246]

Krug SM, Günzel D, Conrad MP, Rosenthal R, Fromm A, Amasheh S, Schulzke JD, Fromm M. Claudin-17 forms tight junction channels with distinct anion selectivity. Cell Mol Life Sci. 2012; 69:2765–78. [PubMed: 22402829]

Li J, Zhuo M, Pei L, Rajagopal M, Yu AS. Comprehensive Cysteine-Scanning Mutagenesis Reveals Claudin-2 Pore-Lining Residues with Different Intrapore Locations. J Biol Chem. 2014; 289:6475–6484. [PubMed: 24436330]

Li J, Zhuo M, Pei L, Yu AS. Conserved aromatic residue confers cation selectivity in claudin-2 and claudin-10b. J Biol Chem. 2013a; 288:22790–7. [PubMed: 23760508]

Li JH, Angelow S, Linge A, Zhuo M, Yu ASL. Claudin-2 pore function requires an intramolecular disulfide bond between two conserved extracellular cysteines. American Journal of Physiology-Cell Physiology. 2013b; 305:C190–C196. [PubMed: 23677799]

Melis MS, Malnic G, Aires MM. Effect of medium tonicity on transepithelial H^+-HCO_3^- fluxes in rat proximal tubule. J Physiol. 1993; 465:9–20. [PubMed: 8229863]

Muto S, Hata M, Taniguchi J, Tsuruoka S, Moriwaki K, Saitou M, Furuse K, Sasaki H, Fujimura A, Imai M, Kusano E, Tsukita S, Furuse M. Claudin-2-deficient mice are defective in the leaky and cation-selective paracellular permeability properties of renal proximal tubules. Proc Natl Acad Sci U S A. 2010; 107:8011–6. [PubMed: 20385797]

Nightingale ER. Phenomenological theory of ion solvation. Effective radii of hydrated ions. J Phys Chem. 1959; 63:1381–1387.

Quigley R, Baum M. Developmental changes in rabbit juxtamedullary proximal convoluted tubule water permeability. Am J Physiol. 1996; 271:871–6.

Rosenthal R, Milatz S, Krug SM, Oelrich B, Schulzke JD, Amasheh S, Günzel D, Fromm M. Claudin-2, a component of the tight junction, forms a paracellular water channel. J Cell Sci. 2010; 123:1913–21. [PubMed: 20460438]

Schafer JA. Transepithelial osmolality differences, hydraulic conductivities, and volume absorption in the proximal tubule. Annu Rev Physiol. 1990; 52:709–26. [PubMed: 2184773]

Schnermann J, Chou CL, Ma TH, Traynor T, Knepper MA, Verkman AS. Defective proximal tubular fluid reabsorption in transgenic aquaporin-1 null mice. Proc Natl Acad Sci USA. 1998; 95:9660–9664. [PubMed: 9689137]

Schnermann J, Huang Y, Mizel D. Fluid reabsorption in proximal convoluted tubules of mice with gene deletions of claudin-2 and/or aquaporin1. Am J Physiol Renal Physiol. 2013; 305:F1352–64. [PubMed: 24049145]

Van Itallie CM, Fanning AS, Anderson JM. Reversal of charge selectivity in cation or anion-selective epithelial lines by expression of different claudins. Am J Physiol Renal Physiol. 2003; 285:1078–84.

Van Itallie CM, Holmes J, Bridges A, Gookin JL, Coccaro MR, Proctor W, Colegio OR, Anderson JM. The density of small tight junction pores varies among cell types and is increased by expression of claudin-2. J Cell Sci. 2008; 121:298–305. [PubMed: 18198187]

Van Itallie CM, Rogan S, Yu A, Vidal LS, Holmes J, Anderson JM. Two splice variants of claudin-10 in the kidney create paracellular pores with different ion selectivities. Am J Physiol Renal Physiol. 2006; 291:1288–99.

Weinstein AM. Transport by epithelia with compliant lateral intercellular spaces: asymmetric oncotic effects across the rat proximal tubule. Am J Physiol. 1984; 247:F848–62. [PubMed: 6496750]

Weinstein AM, Weinbaum S, Duan Y, Du Z, Yan Q, Wang T. Flow-dependent transport in a mathematical model of rat proximal tubule. Am J Physiol Renal Physiol. 2007; 292:F1164–81. [PubMed: 17213461]

Yu AS. Claudins and the Kidney. J Am Soc Nephrol. 2015; 26:11–9. [PubMed: 24948743]

Yu AS, Cheng MH, Angelow S, Günzel D, Kanzawa SA, Schneeberger EE, Fromm M, Coalson RD. Molecular basis for cation selectivity in claudin-2-based paracellular pores: identification of an electrostatic interaction site. J Gen Physiol. 2009; 133:111–27. [PubMed: 19114638]

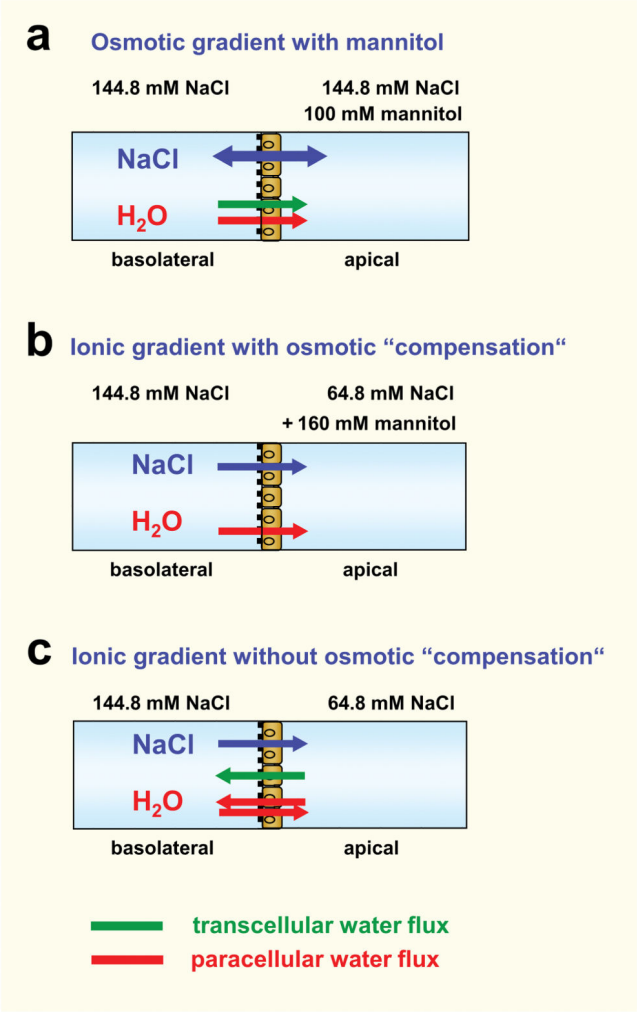

Fig. 1. Experimental conditions for measuring water flow

For measuring water flux the Ussing chamber was filled with HEPES buffered solution with a total NaCl concentration of 144.8 mM. The solution in the apical compartment was changed according to the following conditions: (a) Osmotic gradient with mannitol in the apical compartment. The osmotic gradient with mannitol in the basolateral compartment is not shown here. (b) Ionic gradient with the high NaCl concentration in the basolateral compartment and osmotic "compensation" by mannitol in the apical compartment. As MDCK cells are unable to secrete Na^+, no transcellular Na^+ flux will occur under these conditions. (c) Ionic gradient with the high NaCl concentration in the basolateral compartment and no osmotic "compensation". As in (b) no transcellular Na^+ flux will occur under these conditions. The osmotic and ionic gradients aredirected conversely. Assuming that claudin-2 is the only paracellular water channel, paracellular water flux induced by the ionic gradient will only occur in claudin-2-expressing MDCK I cells. During all experiments the transepithelial potential was clamped at 0 mV. This might favour an isolated paracellular Na^+ passage in claudin-2-expressing cells and thus induce paracellular water flux.

Fig. 2 a

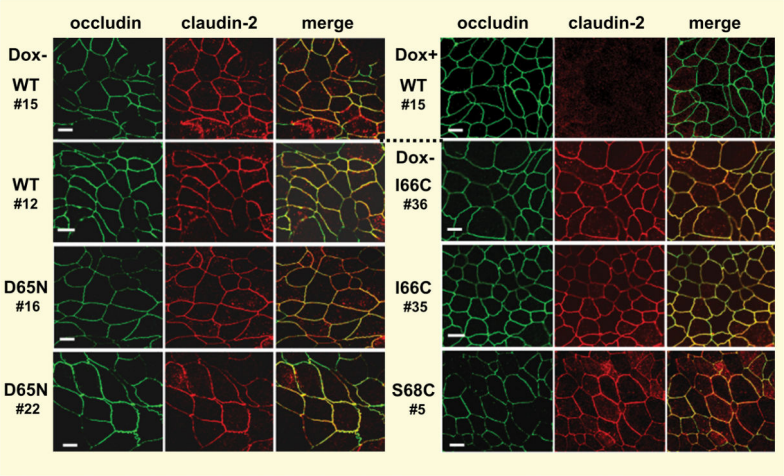

Fig. 2 b

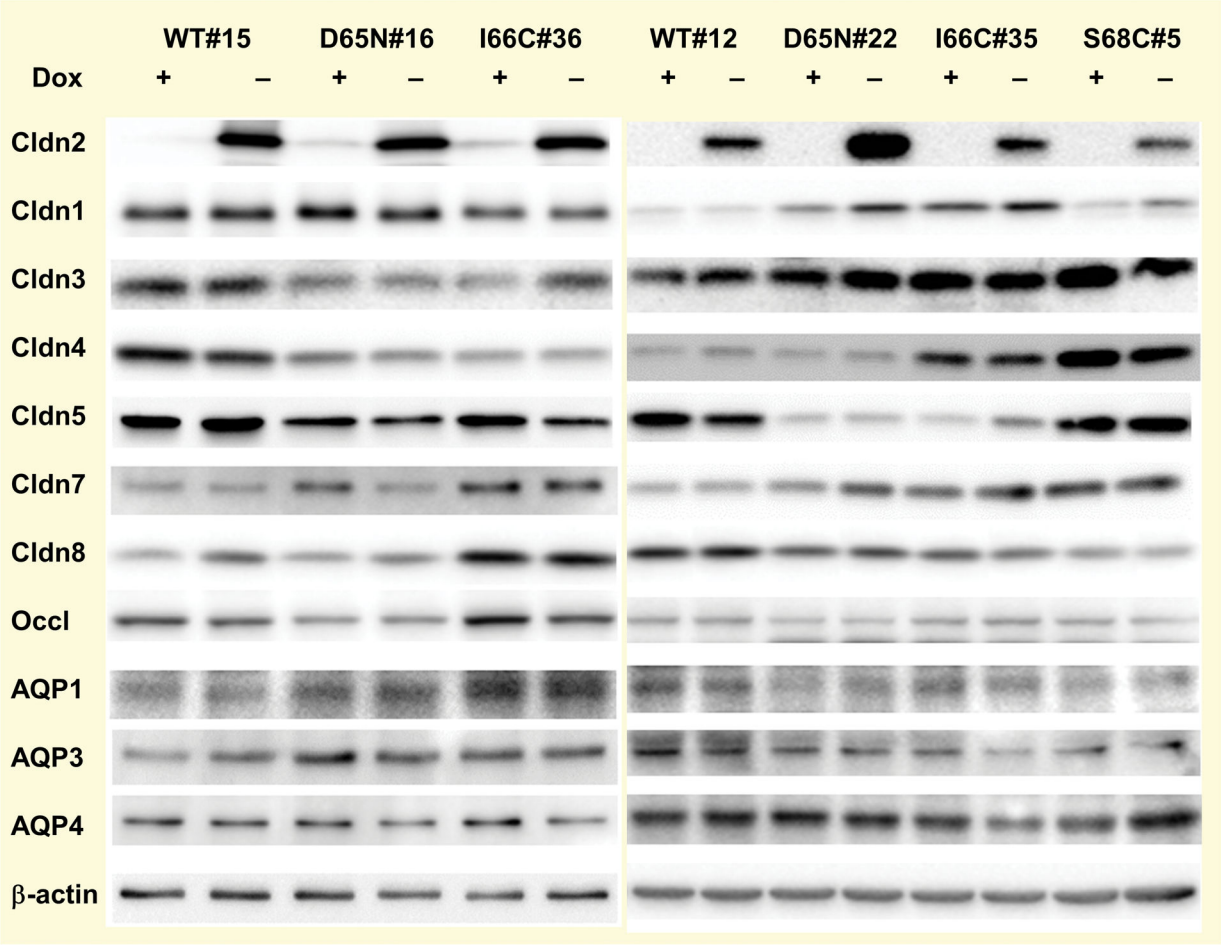

Fig. 2. Tight junction proteins and AQPs in MDCK I TetOff cells stably transfected with mouse wild-type and mutant claudin-2

(a) Subcellular localization of claudin-2 in the cells. Different clones expressing wild-type (WT) claudin-2, and the claudin-2 mutants D65N, and the cysteine mutants I66C and S68C were induced to express claudin-2 (Dox−) and immunofluorescence stained using an antibody against claudin-2 (left) and the tight junction marker occludin (middle). The colocalization of both proteins was confirmed by the merged view (right). No claudin-2 signal could be detected in the uninduced (Dox+) cells, here shown for the uninduced cells of wild-type claudin-2, clone 15. Bar 10 μm. **(b) Claudin and AQP expression in the cells.** Western blot analysis showing the expression of the transfected claudin-2 proteins, endogenous claudins, and aquaporins (AQP) in uninduced (Dox+) and induced (Dox−) MDCK I TetOff cells transfected with wild-type (WT) claudin-2 and the claudin-2 mutants.

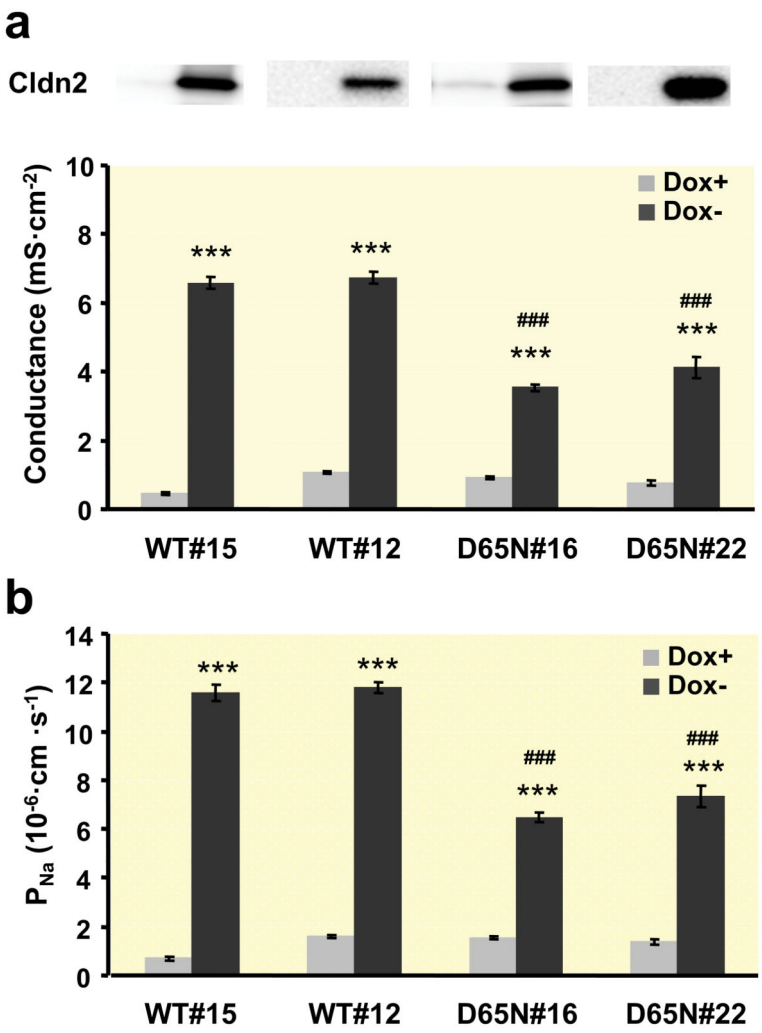

Fig. 3. Electrophysiological properties of MDCK I TetOff cells expressing wild-type or D65N claudin-2

(a) Conductance and **(b)** Na^+ permeability of two different clones of wild-type (WT) and mutated (D65N) claudin-2 (n=7–14). The upper panel in (A) is a Western blot (from Fig. 2b) showing claudin-2 protein expression in each clone (left lane, Dox+; right lane, Dox−). Permeability was derived from measurement of dilution potentials and calculated by means of the Goldman-Hodgkin-Katz equation. As expected, a strong difference in conductance and permeability could be observed between induced (Dox−) and uninduced (Dox+) cells and also between cells expressing wild-type and mutated claudin-2. (*** $p < 0.001$ vs. Dox +, ### $p < 0.001$ vs. WT#12 and WT#15).

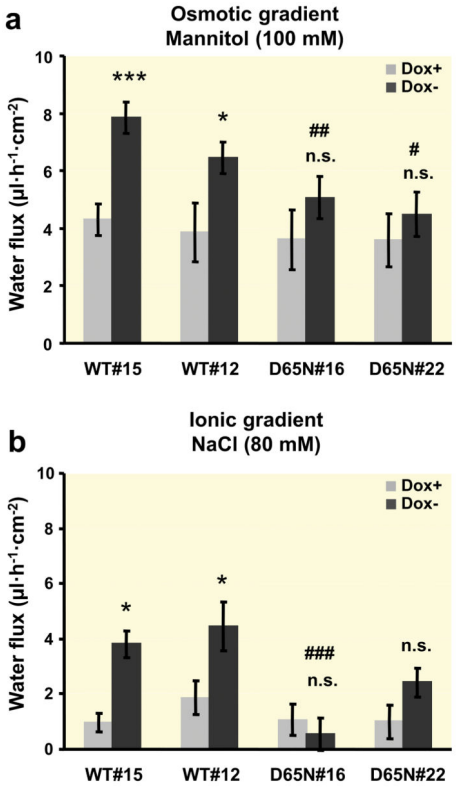

Fig. 4. Water flux across layers of MDCK I TetOff cells expressing wild-type or D65N claudin-2

(a) Water flux induced by an osmotic gradient with 100 mM mannitol on the apical side of the cell layer (n=7–12). **(b)** Water flux induced by an ionic gradient with a difference of 80 mM NaCl and the high NaCl concentration at the basolateral side of the cell layer. The osmotic difference was compensated by the addition of 160 mM mannitol to the apical side (n=6–13). Positive water flux is defined as flow from basolateral to apical side. In the wild-type claudin-2-transfected cells, water flux was increased in the induced Dox− cells compared to the uninduced Dox+ cells under both osmotic and ionic gradients, whereas no difference could be observed in D65N claudin-2-transfected cells. (*$p < 0.05$, ***$p < 0.001$, n.s. = not significant vs. Dox+; # $p < 0.05$ vs. WT#12 and WT#15, ## $p < 0.01$ vs. WT#15, ### $p < 0.001$ vs. WT#15 and WT#12).

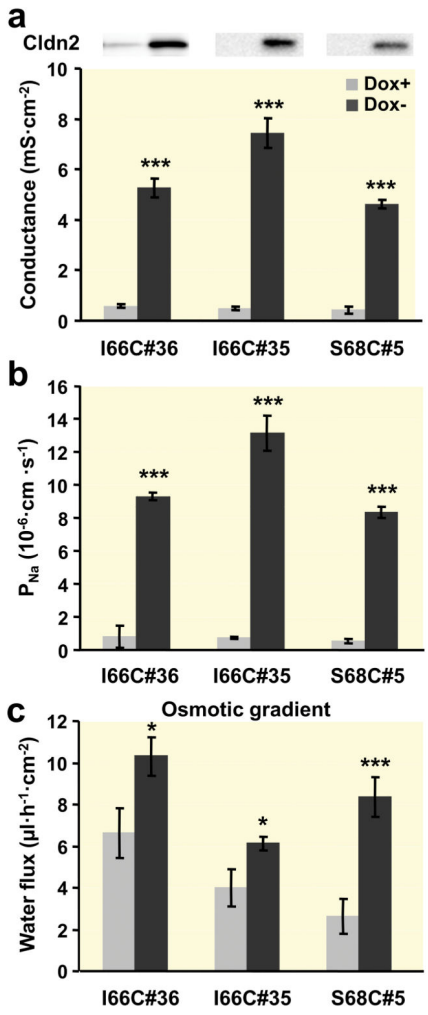

Fig. 5. Characterization of MDCK I TetOff cells stably transfected with claudin-2 cysteine mutants

(a) Conductance, **(b)** Na^+ permeability, and **(c)** osmotic gradient-induced water flux (100 mM mannitol at the apical side) of two different clones of I66C and one clone of S68C claudin-2 mutants (n=7–14). The upper panel in (A) is a Western blot (from Fig. 2b) showing claudin-2 protein expression in each clone (left lane, Dox+; right lane, Dox−). Permeability was derived from measurement of dilution potentials and calculated by means of the Goldman-Hodgkin-Katz equation. Conductance, Na^+ permeability, and water flux were all increased in induced (Dox−) cells. (* $p < 0.05$, *** $p < 0.001$ vs. Dox+).

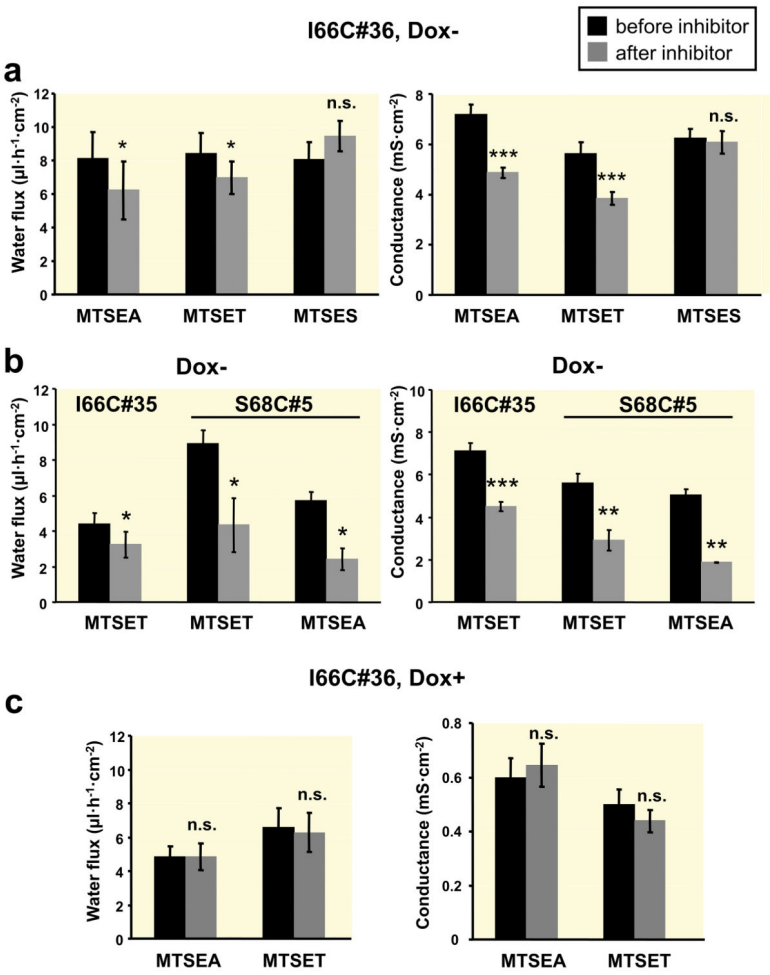

Fig. 6. Effects of MTS reagents on water flux and conductance in MDCK I TetOff cells expressing claudin-2 cysteine mutants

Osmotic gradient-induced water transport (left panel) and conductance (right panel) before and after addition of different MTS reagents ("inhibitor") in induced (Dox−, **a, b**) and uninduced (Dox+, **c**) MDCK I TetOff cells expressing I66C claudin-2 (#36), and in induced (Dox−, **b**) cells expressing I66C (#35) and S68C (#5) claudin-2 (n=4–10). MTSEA (2.5 mM) and MTSET (1 mM) caused a decrease in water flux and conductance in Dox− cells of all mutants, whereas MTSES (5 mM) had no effect on either conductance or water flux. MTSEA and MTSET did not exert any effect on Dox+ cells. (n.s. = not significant, * $p < 0.05$, ** $p < 0.01$, *** $p < 0.001$ vs. before inhibitor, paired Student's *t* test).

Fig. 7 a

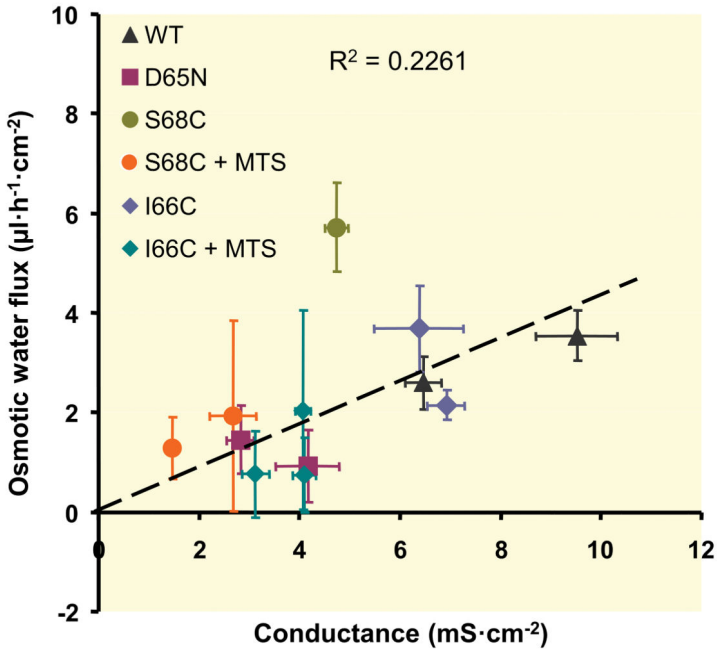

Fig. 7 b

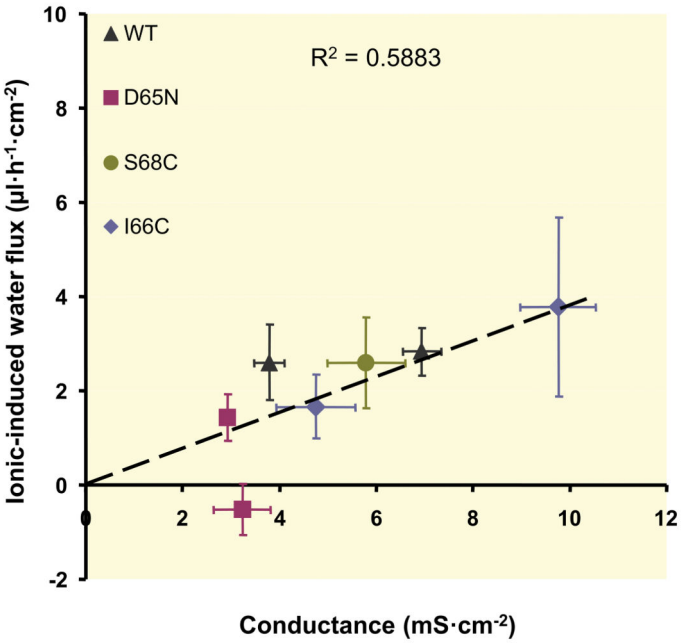

Fig. 7. Relationship between claudin-2-mediated water flux and claudin-2-mediated conductance

The water flux mediated by claudin-2 was calculated as the difference between water flux of uninduced (Dox+) and induced (Dox−) cells. Claudin-2 conductance was calculated as the difference between conductance of uninduced (Dox+) and induced (Dox−) cells. Each data point represents the values (mean ± SEM) determined in one clonal cell line. Decrease in conductance due to charge neutralization (D65N), blocking of the claudin-2 pore with MTS reagents (only in **a**), or clonal variation, are all associated with a commensurate decrease in water flux. The dashed line was fitted by linear regression to all data points. **(a)** Relationship between osmotic-induced water flux and conductance, slope 0.336 $\mu l \cdot h^{-1} \cdot mS^{-1}$. **(b)** Relationship between water flux induced by the NaCl gradient (ionic-induced water flux) and conductance, slope 0.436 $\mu l \cdot h^{-1} \cdot mS^{-1}$.

Table 1

Characteristics of MDCK I TetOff cells stably transfected with wild-type and mutant claudin-2

Data of conductance and permeability data have been obtained from dilution potential measurements in the Ussing chamber and corrected for filter and fluid resistance (n=6–14). Water flux measurements were performed in the modified Ussing chamber with water flux induced by an osmotic gradient (100 mM mannitol apical, n=7–14, or *basolateral, n=3–11) or ionic gradient (NaCl difference 80 mM, high NaCl basolateral, 160 mM mannitol apical, n=4–13 or ** NaCl difference 80 mM, high NaCl basolateral, without mannitol at the apical side, n=6–8). Water flux from the apical to the basolateral side is indicated by a negative prefix. Water permeability was calculated from $P_{water} = J/\Delta c$ with P = permeability (cm s^{-1}), J = flux (mol·h^{-1}·cm^{-2}), and c = concentration (mol/l). P_{water} mediated by claudin-2 was 4.73 10^{-4} cm s^{-1} and 1.83 10^{-4} cm s^{-1} for wildtype and D65N claudin-2, respectively

MDCK I TetOff claudin-2		Conductance mS·cm^{-2}		P_{Na} 10^{-6}cm·s^{-1}		P_{Cl} 10^{-6}cm·s^{-1}		P_{Na}/P_{Cl}		Water flux µl·h^{-1}·cm^{-2}				P_{water} 10^{-4}cm·s^{-1}	
										osmotic		ionic			
		mean	SEM	mean	SEM	mean	SEM	mean	SEM	mean	SEM	mean	SEM	mean	SEM
WT#15	Dox+	0.45	0.05	0.71	0.08	0.21	0.03	3.63	0.36	4.31 −4.57*	0.55 0.73*	0.97 −2.05**	0.33 0.93	6.65	0.85
	Dox−	6.57	0.17	11.58	0.34	0.96	0.06	12.45	1.11	7.85 −8.23*	0.55 0.74*	3.80 −2.11**	0.49 0.69	12.11	0.85
WT#12	Dox+	1.08	0.04	1.61	0.06	0.58	0.04	2.83	0.16	3.86	1.03	1.87	0.62	5.96	1.59
	Dox−	6.73	0.17	11.80	0.22	1.02	0.14	13.21	2.68	6.46	0.55	4.47	0.88	9.97	0.85
D65N#16	Dox+	0.91	0.03	1.53	0.05	0.32	0.02	5.00	0.26	3.61	1.04	1.07 −5.94**	0.58 1.67	5.57	1.6
	Dox−	3.54	0.09	6.47	0.18	0.52	0.05	13.84	1.46	5.06	0.74	0.55 −5.30**	0.58 1.19	7.81	1.14
D65N#22	Dox+	0.75	0.07	1.38	0.09	0.15	0.06	12.71	1.91	3.57	0.92	0.99	0.62	5.51	1.42
	Dox−	4.13	0.30	7.33	0.44	0.76	0.20	17.06	3.69	4.49	0.76	2.42	0.53	6.93	1.17
I66C#36	Dox+	0.59	0.09	0.79	0.66	0.41	0.08	2.22	0.24	6.64 −7.89*	1.20 0.93*	3.46	0.67	10.25	1.85
	Dox−	5.28	0.38	9.28	0.23	0.91	0.22	15.24	3.33	10.32 −12.24*	0.92 0.51*	5.12	0.66	15.93	1.42
I66C#35	Dox+	0.49	0.06	0.71	0.07	0.29	0.05	2.83	0.29	3.99	0.90	1.18	1.76	6.16	1.39

MDCK I TetOff claudin-2		Conductance mS·cm^{-2}		P_{Na} 10^{-6}cm·s^{-1}		P_{Cl} 10^{-6}cm·s^{-1}		P_{Na}/P_{Cl}		Water flux µl·h^{-1}·cm^{-2} osmotic		ionic		P_{water} 10^{-4}cm·s^{-1}	
		mean	SEM	mean	SEM	mean	SEM	mean	SEM	mean	SEM	mean	SEM	mean	SEM
S68C#5	Dox−	7.44	0.61	13.13	1.05	0.85	0.16	21.99	4.41	6.14	0.32	4.96	2.09	9.48	0.49
	Dox+	0.42	0.12	0.53	0.15	0.33	0.13	1.91	0.18	2.64	0.82	−1.47	1.11	4.07	1.27
	Dox−	4.62	0.17	8.32	0.34	0.69	0.10	15.59	3.99	8.35	0.93	1.12	0.96	12.89	1.44

Table 2
Morphometric analysis of tight junction ultrastructure

Tight junction ultrastructure was analyzed using freeze-fracture electron microcopy (*p < 0.05 versus uninduced (Dox+) cells). The analysis between the groups Dox+ and Dox− was blinded

	WT#15 Dox+	WT#15 Dox−	D65N#16 Dox+	D65N#16 Dox−
(n)	(7)	(10)	(13)	(12)
Number of horizontal strands	4.14 ± 0.46	3.50 ± 0.22	3.75 ± 0.25	4.31 ± 0.41
Vertical meshwork depth (nm)	204.3 ± 42.8	196.0 ± 33.0	229.6 ± 37.3	228.1 ± 33.5
Breaks per μm strand length	0.06 ± 0.06	0.14 ± 0.10	0.02 ± 0.02	0.09 ± 0.05
Particle-type/continuous strands %	29/71	70/30*	17/83	46/54*